How to cite: *Angew. Chem. Int. Ed.* **2024**, e202408670
doi.org/10.1002/anie.202408670

Polymer Chemistry | Hot Paper

Self-Adaptive Synthesis of Non-Covalent Crosslinkers while Folding Single-Chain Polymers

*Dawei Qi, Xuncheng Shi, Caihong Lin, Ferdinand Holzhausen, Liljeström Ville, Xun Sun, Jinghui Luo, Leena Pitkänen, Ya Zhu, Jessica Rosenholm, Sirpa Jalkanen, and Jianwei Li**

Abstract: Peptide folding is a dynamic process driven by non-covalent cross-linking leading to functional nanostructures for essential biochemical activities. However, replicating this process in synthetic systems is challenging due to the difficulty in mimicking nature's real-time regulation of non-covalent crosslinking for single-chain polymer folding. Here, we address this by employing anionic dithiol building blocks to create macrocyclic disulfides as non-covalent crosslinkers that adapted to the folding process. Initially, small macrocycles facilitated a low degree folding of a polycation. Then, this preorganized structure catalysed the production of larger macrocycles that enhanced the folding conversely. The self-adaptive synthesis was verified through the encapsulation of an anticancer drug, showing an updated production distribution of non-covalent crosslinkers and maximizing drug-loading efficiency against drug-resistant cancer in vitro. Our research advances the understanding of molecular systems by exploring species evolution via the structural dynamics of polymer folding. Additionally, adaptive synthesis enables controlled, sequential folding of synthetic polymers, with the potential to mimic protein functions.

Introduction

Peptide folding, mediated by non-covalent interactions, plays a crucial role in vital biological processes including enzyme catalysis, transmembrane protein transport, and antigen binding.[1] This has inspired the bionic folding of synthetic polymers using crosslinkers to non-covalently drive the association with recognition sites on the polymer.[2] However, the challenge arises because these non-covalent crosslinkers typically have a fixed chemical structure, whilst the molecular environment around their binding sites varies during folding, leading to unpredictable association strengths with the polymer. Consequently, the use of static crosslinkers hinders efficient control over the folding process.

In contrast, Nature utilises a more sophisticated strategy to facilitate folding performance. In natural systems, the structure of non-covalent crosslinkers for peptide folding is regulated in real-time, corresponding to the progress of folding. For instance, certain molecular chaperones act as transient non-covalent crosslinkers, binding with peptides to promote conformational changes and stabilise folding intermediates.[3] These chaperones are then downregulated to allow for the binding of successor molecules. Furthermore, post-translational modifications are introduced at specific times to modify the intra-peptide non-covalent interactions, guiding the folding towards the correct outcome.[4] Absent these structural adaptations, proteins may misfold or aggregate, leading to dysfunction. This highlights the significance of crosslinker structural adaption in precise folding control, and has inspired the development of hetero-functional polymers and orthogonal crosslinking chemistries to improve the control over the folding process.[5] However, these prefabricated crosslinkers have not yet successfully emulated the timely adaptation seen in natural processes.

Here, we present self-regulating systems from which the synthesis of non-covalent crosslinkers can autonomously

[*] D. Qi, X. Shi, C. Lin, F. Holzhausen, S. Jalkanen, J. Li
MediCity Research Laboratory
University of Turku
Tykistökatu 6, FI-20520 Turku, Finland
E-mail: jianwei.li@utu.fi

L. Ville
Nanomicroscopy Center, OtaNano
Aalto University
Espoo, 00076, Aalto, Finland

X. Sun, J. Luo
Paul Scherrer Institut
Forschungsstrasse 111, 5232 Villigen PSI, Switzerland

L. Pitkänen, Y. Zhu
Department of Bioproducts and Biosystems
Aalto University
02150 Espoo, Finland

J. Rosenholm
Pharmaceutical Sciences Laboratory, Faculty of Science and Engineering
Åbo Akademi University
20500 Turku, Finland

adapt in response to the simultaneous folding process of synthetic polymers. Our self-adaptive synthesis for exploring supramolecular single-chain nanoparticles (Supra-SCNPs) is achieved by dynamic combinatorial chemistry (DCC).[6] DCC relies on reversible chemical reactions that link building blocks combinatorically to generate mixtures of products. The inherent reversibility of the reaction allows the products to exchange components, thereby giving rise to a dynamic combinatorial library (DCL) of interconverting molecules. The concentration distribution of library members is typically under thermodynamic control. This suggests that the introduction of stimuli into the library can influence the stability of library species, consequently altering the composition of the library. Template molecules have been used to shift the equilibrium by amplifying the concentration of the species that have strong affinity with the template, while consuming the species with weak affinity. Unfortunately, almost all the previous template effects are triggered by small molecules of which conformation remains nearly the same during the equilibrating process. This static behaviour amplifies library species simply based on the binding with recognition sites, preventing discovering new template effects enriched by in situ dynamics like responsive conformational changes. Though some pioneering work has utilized proteins,[7] nucleic acids[8] or even cells[9] as templates for the study of DCC, they were mostly regarded as well-organized static targets. The contribution from their possible conformational dynamics of macromolecules had been rarely studied.

Polymer folding is such a dynamic process governed by thermodynamics, where the polymer progresses through intermediate states to its most stable structure.[10] When the folding is driven by a DCL of non-covalent crosslinkers, these varying conformational states create diverse molecular environments, which directs the spontaneous amplification of the suitable non-covalent crosslinkers that have strong respective association with the folding polymer at each state. This amplification assists the polymer in overcoming transitional states to achieve stability. Moreover, the time-dependent nature of folding allows real-time observation and understanding on the evolution of library species, aiding control over the folding process by manipulating dynamic covalent reactions within the library. Therefore, in this study, we synchronise polymer folding with self-adaptive synthesis from DCLs. This integration advances the field of DCC by exploring species evolution directed by the structural dynamics of folding polymers. It simultaneously opens avenues for achieving and controlling stepwise folding of synthetic polymers into Supra-SCNPs, potentially mirroring the functionality of proteins.

Results and Discussion

Distinctive Synthetic Outcome of Non-Covalent Crosslinkers after Folding the Polymers

For the fabrication of DCLs that enable the synthesis of dynamic combinatorial non-covalent crosslinkers, aimed at directing the folding of polymeric templates, we initiated our approach by synthesizing a linear cationic homopolymer, poly[3-(methacryloylamino)propyl]trimethyl ammonium chloride ($\mathbf{PT}_{703}$, Figure 1A), to serve as the folding scaffold. The inherent positive charge of the monomer predisposes the polymer at a stretched nascent conformation when in an aqueous solution, priming it for subsequent folding. The obtained polymer was characterized by proton nuclear magnetic resonance spectroscopy (^{1}H NMR, Figure S1) and size exclusion chromatography (Figure S2, Table S1). In the next step, we synthesized a benzoic dithiol building block, labelled **A**, featuring a carboxylic acid group (Figure 1A, Figure S3 and S4).[11] Upon deprotonation under physiological conditions, **A** acquires a negative charge and its thiol groups can be oxidized into disulfide bonds to yield macrocyclic species $\mathbf{A}_n$, which function as potential non-covalent crosslinkers for polymer folding. The interaction between $\mathbf{A}_n$ and $\mathbf{PT}_{703}$'s pendants, leading to charge neutralization, triggers the polymer's folding through hydrophobic effect.

Subsequently, two DCLs were made from **A** (3.00 mM) without and with the polymeric template $\mathbf{PT}_{703}$ (15.00 mM, in monomer) in phosphate buffer at pH 7.4. In accordance with the concentration of **A** and $\mathbf{PT}_{703}$, the two DCLs were named as 3**A** and 3**A**-15$\mathbf{PT}_{703}$, respectively. The high-performance liquid chromatography (HPLC) spectra of the DCLs showed no noticeable changes two weeks after preparation. Even after one year, re-examination of the library revealed undetectable changes, indicating the chemical equilibrium of the $\mathbf{A}_n$ distribution remained stable. The HPLC-mass spectroscopy (HPLC-MS) analysis of the two equilibrated libraries suggested that the presence of $\mathbf{PT}_{703}$ significantly supressed the production of $\mathbf{A}_4$, while amplifying the production of the group of larger macrocycles ranging from the heptamer ($\mathbf{A}_7$) to the hendecamer ($\mathbf{A}_{11}$) (Figure 2A, Figure S5–S9). However, the HPLC-MS analysis of a control library prepared from **A** (3.00 mM) and a small molecular template **ST** (15.00 mM) (Figure 1A, Figure S10), an analogue to the pendant of $\mathbf{PT}_{703}$, showed a similar spectrum as the library 3**A** (Figure S11). These results suggested that the polymeric template exhibited a unique template effect, which was not achievable with the monomeric template, even if it had the same recognition site.

This evident template effect encouraged us to verify whether $\mathbf{PT}_{703}$ was bound with and folded by the $\mathbf{A}_n$ with various sizes using diffusion-ordered ^{1}H NMR spectroscopy (DOSY). In the DOSY two-dimensional (2D) plot of the fully oxidised 3**A**-15$\mathbf{PT}_{703}$ library, the ^{1}H NMR signal from both $\mathbf{A}_n$ and $\mathbf{PT}_{703}$ were broadened and in alignment at a same diffusion coefficient (D), indicating their quantitative supramolecular complexation (Figure 2B). The D of the supramolecular complex was larger than that of the 15.00 mM $\mathbf{PT}_{703}$ (15$\mathbf{PT}_{703}$) alone. By converting D to hydrodynamic radius (R_h) using Stokes–Einstein equation, a decreased R_h from ~6.86 nm of 15$\mathbf{PT}_{703}$ to ~4.67 nm of 3**A**-15$\mathbf{PT}_{703}$ was shown, suggesting folding of $\mathbf{PT}_{703}$. Moreover, we determined the radius of gyration (R_g) of the polymer by Guinier analysis based on small angle X-ray scattering (SAXS) measurement, and compactness of the polymer by

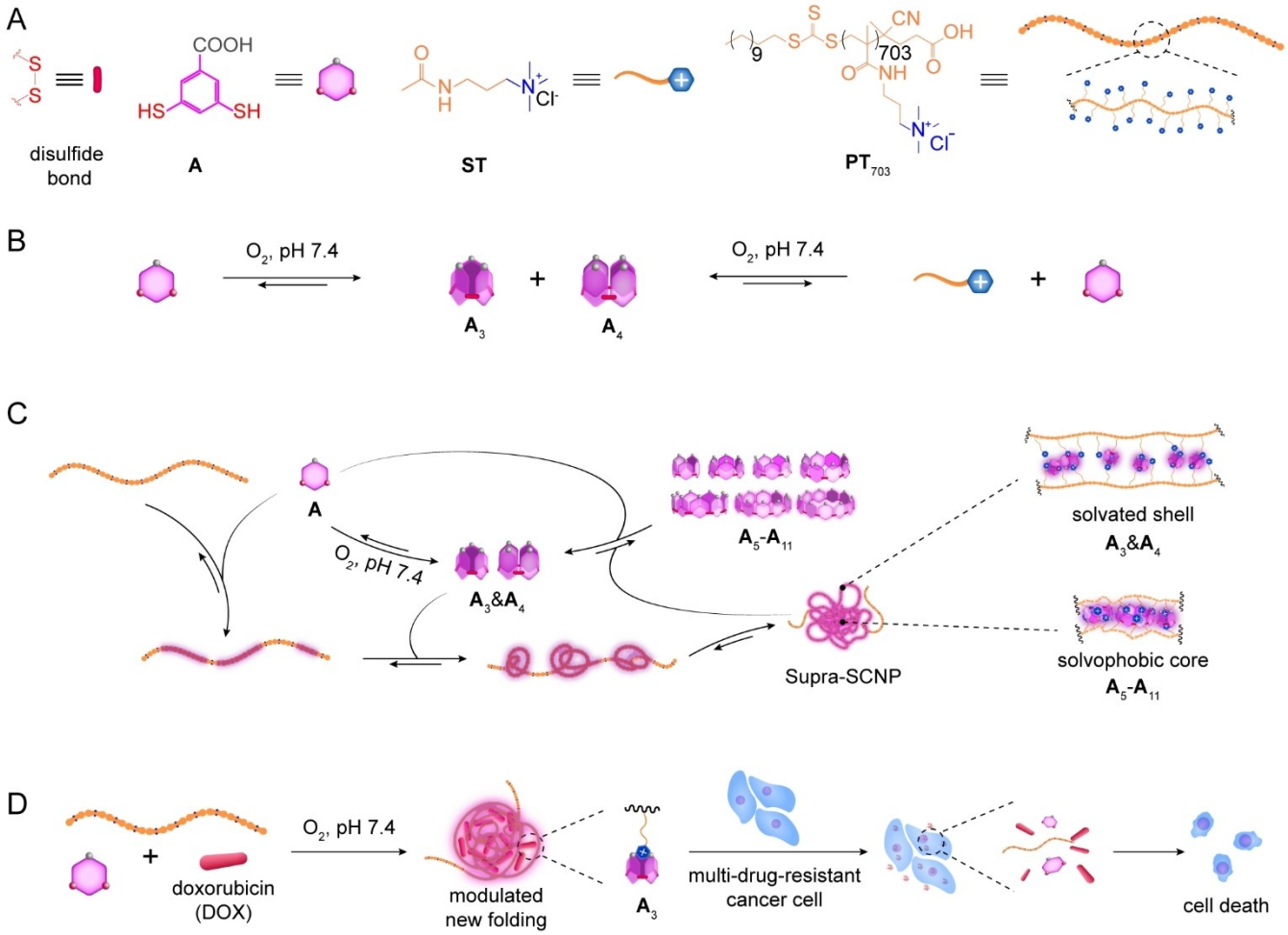

Figure 1. (**A**) Chemical structures and cartoon representations of the building block **A**, small molecular template **ST** and polymeric template $\mathbf{PT}_{703}$. (**B**) Schematic of blank DCL made by **A** alone, and control DCL made by **A** and **ST** to clarify if there were independent interactions between **A** and **ST**. (**C**) Schematic of the synthesis of macrocyclic non-covalent crosslinkers adapting in real-time to the folding process of polymeric template in the DCL made by **A** and $\mathbf{PT}_{703}$. **A** formed supramolecular complex with $\mathbf{PT}_{703}$ quantitatively. Then **A** oxidized into $\mathbf{A}_3$&$\mathbf{A}_4$ to help the complex fold into a transient intermediate state. Concurrently, $\mathbf{A}_3$&$\mathbf{A}_4$ converted into $\mathbf{A}_5$-$\mathbf{A}_{11}$ to maximize the folding. In the finalized folding, $\mathbf{A}_3$&$\mathbf{A}_4$ located in the solvated loosely folded outer shell, $\mathbf{A}_5$-$\mathbf{A}_{11}$ located in the solvophobic tightly folded inner core. (**D**) Schematic of DOX modulating the folding outcome and the adaptive synthesis of crosslinkers. $\mathbf{A}_3$ was dominantly synthesized to enlarge the folding for encapsulating more DOX. The obtained molecular complex could work as drug delivery system against drug-resistant cancer cells in vitro.

transverse NMR relaxation time (T_2) by ^{1}H NMR . In principle, smaller R_g represents smaller root mean square distance from the monomers to the polymer's centre of the mass. Shorter T_2 is an indicator of a more compact micro-environment around the molecule.[12] Indeed, $\mathbf{PT}_{703}$ had significantly smaller R_g and shorter T_2 in the 3**A**-15$\mathbf{PT}_{703}$ library than it alone (Figure 2C, Figure S12), confirming the polymer folding by $\mathbf{A}_n$. In addition, D and T_2 of the library no longer changed observably after the chemical equilibrium, indicating a dual equilibrium between polymer folding and DCC. Lastly, the transmission electron microscopy (TEM) and dynamic light scattering (DLS) analysis showed that the supramolecular single chain nanoparticles (Supra-SCNPs) in 3**A**-15$\mathbf{PT}_{703}$ library were compact globules with an average radius of 7.5 nm (Figure 2D and inset), which was consistent with that determined by R_h and R_g.

All together, these results confirmed that $\mathbf{PT}_{703}$ was successfully folded into Supra-SCNPs by $\mathbf{A}_n$ synthesized from the 3**A**-15$\mathbf{PT}_{703}$ library. The unique template effect in the DCLs suggested a possible structural adaptation of $\mathbf{A}_n$ to the chemical environments emerged from the folding.

Chemical Environments around the Non-Covalent Crosslinkers in the Supra-SCNPs

Given that polymer folding is propelled by hydrophobic compaction — a process that potentially diminishes the dynamism of involved motifs — we sought to identify these environments through the assessment of molecular dynamics (expressed as D and T_2) via ^{1}H NMR . Unfortunately, the ^{1}H NMR signals for $\mathbf{A}_n$ species initially coalesced, but separation was achieved by incorporating 30 % CD_3CN by

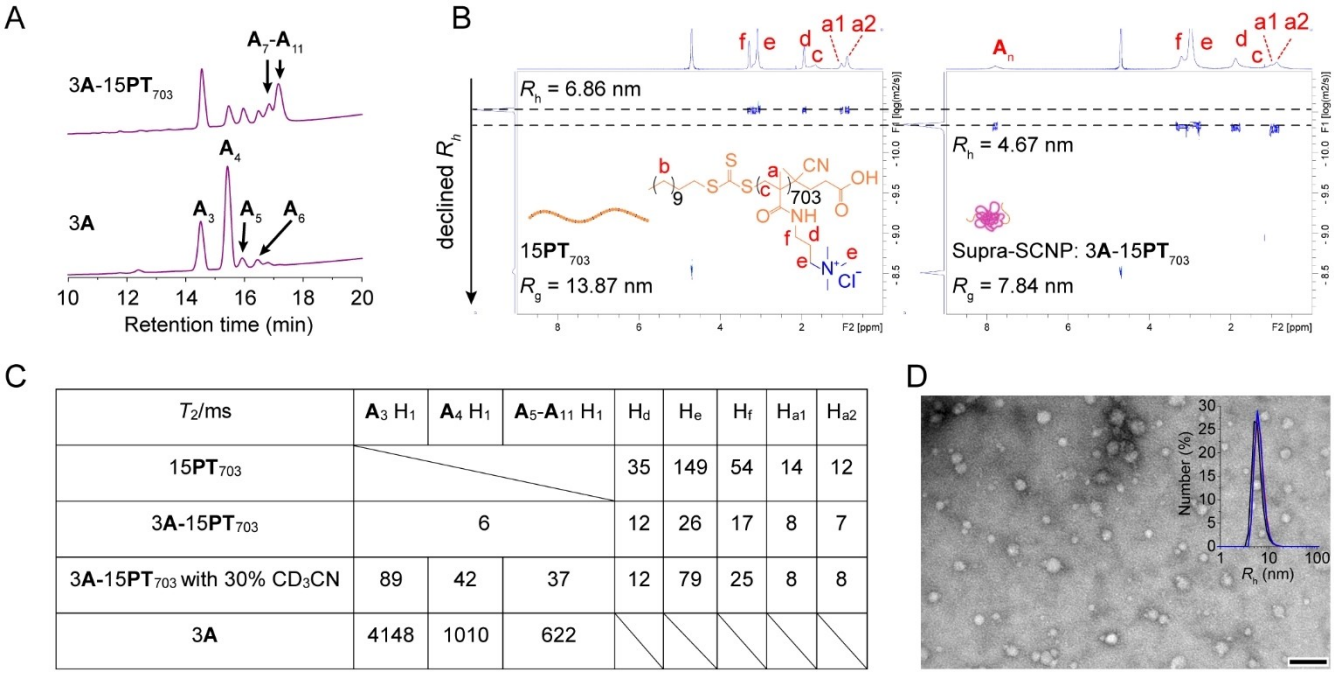

T_2/ms	A_3 H_1	A_4 H_1	A_5-A_{11} H_1	H_d	H_e	H_f	H_{a1}	H_{a2}
15PT703				35	149	54	14	12
3A-15PT703	6			12	26	17	8	7
3A-15PT703 with 30% CD_3CN	89	42	37	12	79	25	8	8
3A	4148	1010	622					

Figure 2. (**A**) HPLC spectra assigned by MS of the blank library 3**A** (3.00 mM **A**) and the Supra-SCNP-synthesizing library 3**A**-15**PT**$_{703}$ (equilibrated from mixing 3.00 mM **A** and **PT**$_{703}$ with 15.00 mM cationic pendants) made in phosphate buffer at pH 7.4. (**B**) DOSY 2D plots of the solutions of 15**PT**$_{703}$ (left, polymer alone with 15.00 mM cationic pendants) and the equilibrated library of 3**A**-15**PT**$_{703}$ (right). Both samples were prepared in deuterated phosphate buffer (pD 7.4). The *D* was smaller higher up in the y-axis, meaning larger hydrodynamic size. (**C**) T_2 relaxation times of the DCLs measured by the CPMG NMR experiments on a 600 MHz NMR spectrometer. All the samples were in the same phosphate buffer at pD 7.4. (**D**) TEM image observing the Supra-SCNP emerged from the 3**A**-15**PT**$_{703}$ (3.00 mM **A** and **PT**$_{703}$ with 15.00 mM cationic pendants), scale bar 100 nm. Inset: Number-averaged distribution of hydrodynamic radius (R_h) of 3**A**-15**PT**$_{703}$ analysed by DLS.

volume in D_2O. This adjustment enabled precise assignment of the H_1 and H_2 signals for $\mathbf{A}_3$, $\mathbf{A}_4$, and the coalesced $\mathbf{A}_5$-$\mathbf{A}_{11}$ species, corroborated by DOSY (Figure 3A, Figure S13A), ^{1}H-^{1}H TOCSY (Figure S13B), and cross-referenced with HPLC data (Figure S13C). It is worth noting that the addition of CD_3CN preserved the supramolecular interaction within the Supra-SCNPs, as evidenced by the comparative T_2 values of $\mathbf{A}_n$ and **PT**$_{703}$ (Figure 2C), and Nuclear Overhauser Effect (NOE) correlations between $\mathbf{A}_n$ and **PT**$_{703}$ in the ^{1}H-^{1}H NOESY 2D plot (Figure 3B).

The discrimination of the NMR spectral peaks corresponding to different non-covalent crosslinkers facilitated the elucidation of their respective chemical environments via molecular dynamics. DOSY plots revealed that species $\mathbf{A}_5$-$\mathbf{A}_{11}$ aligned with **PT**$_{703}$, in contrast to $\mathbf{A}_3$ and $\mathbf{A}_4$ which exhibited greater diffusion coefficients. This gradation in T_2 values from $\mathbf{A}_3$ and $\mathbf{A}_4$ to $\mathbf{A}_5$-$\mathbf{A}_{11}$ (Figure 2C) intimates a deceleration in diffusion, indicative of three discrete chemical environments distinguished by their increasing degrees of spatial compactness. Crucially, $\mathbf{A}_3$ and $\mathbf{A}_4$ demonstrated marked NOE interactions with water protons (Figure S14), suggesting their localization within the hydrated shell of the Supra-SCNP. Thus, our findings categorize two primary chemical environments within the Supra-SCNPs, delineated by the compactness and specific binding locales: $\mathbf{A}_3$ and $\mathbf{A}_4$ were associated with more open binding sites within the hydrated shell, whereas $\mathbf{A}_5$-$\mathbf{A}_{11}$ were localized to the compacted binding sites within the hydrophobic core (Figure 3C).

The Adaptation Mechanism of Non-Covalent Crosslinkers in the Identified Chemical Environments

Incorporating this identified spatial distribution and the concentration distribution of library species, we hypothesized that the adaptive synthesis of $\mathbf{A}_n$ molecules was influenced by the increasing spatial compactness from the shell to the core of the Supra-SCNP. This gradation in compactness led to an augmented local effective concentration of $\mathbf{A}_n$ due to volumetric compaction. Guided by Le Chatelier's principle,[13] which posits that an equilibrium system will adjust to minimize concentration changes, we anticipated a reduction in the number of core macrocycles through enhanced conversion into larger macrocycle variants.

To validate the implications of Le Chatelier's principle, we initially established a series of control DCLs without any template, utilizing variable concentration of **A**, to observe its influence on $\mathbf{A}_n$'s distribution via HPLC analysis (Figure 3D). With increasing **A**'s concentration, a pronounced trend favouring the formation of larger macrocycles ($\mathbf{A}_7$-$\mathbf{A}_{11}$) over smaller ones ($\mathbf{A}_3$ and $\mathbf{A}_4$) was noted.

Further investigation assessed whether this principle could elucidate the observed preferential amplification of

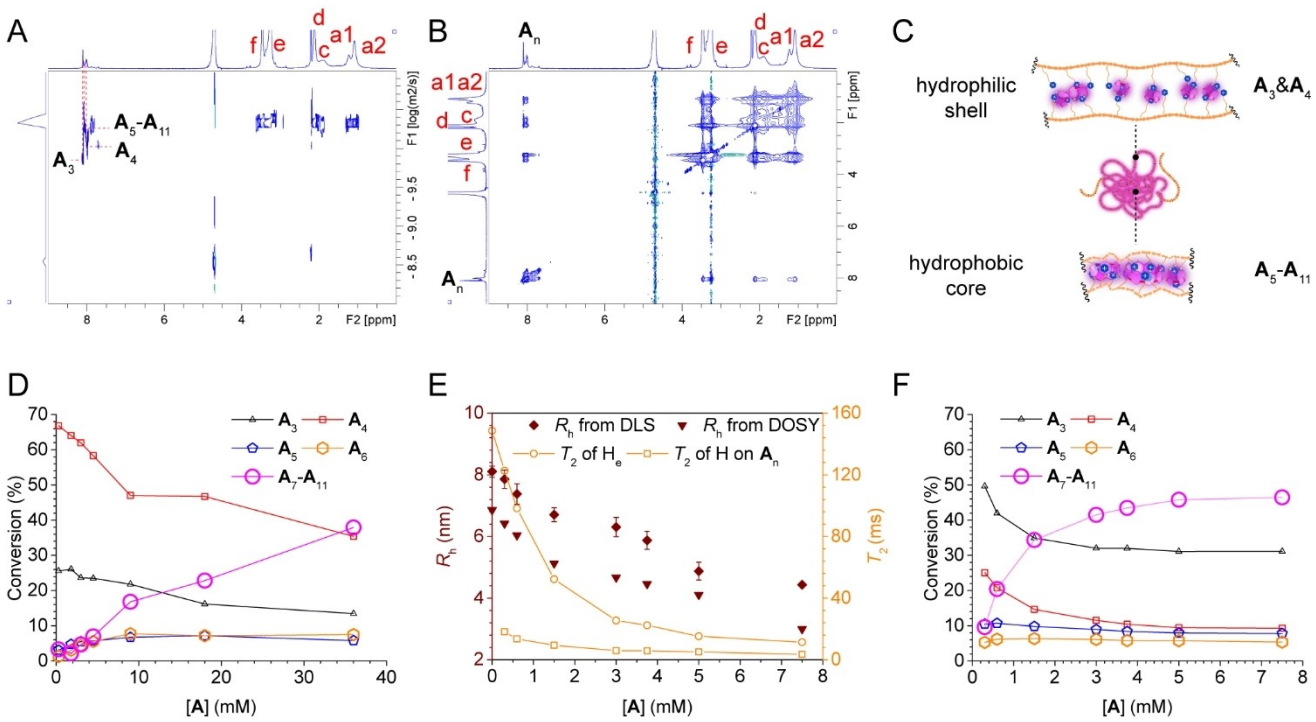

Figure 3. (**A**) DOSY 2D plot and (**B**) NOESY 2D plot of a 3**A**-15**PT**$_{703}$ DCL equilibrated in the phosphate buffer prepared by D_2O and CD_3CN in 7 : 3 volume ratio at pD 7.4. (**C**) Schematic of the inner-Supra-SCNP chemical environments and the different $\mathbf{A}_n$ adapted within. In the hydrophobic core, the polymer was densely folded, the bound $\mathbf{A}_n$ adapted to its larger form of $\mathbf{A}_5$-$\mathbf{A}_{11}$. In the hydrophilic shell, the polymer was loosely folded, the bound $\mathbf{A}_n$ adapted to its smaller form of $\mathbf{A}_3$ and $\mathbf{A}_4$. (**D**) Conversion of **A** to different subset of $\mathbf{A}_n$ in the equilibrated control n**A** DCLs at different concentration of **A** without any template. (**E**) T_2 and R_h of the equilibrated Supra-SCNPs from the n**A**-15**PT**$_{703}$ DCLs with 15 mM **PT**$_{703}$ and different concentrations of **A**. The error bars in DLS analysis was showing standard errors for triplicate experiments. (**F**) Conversion of **A** to different subset of $\mathbf{A}_n$ in the equilibrated n**A**-15**PT**$_{703}$ DCLs, from the same batch of samples used in (**E**).

larger macrocycles in the context of the folding polymer **PT**$_{703}$. By modulating the degree of polymer folding to enhance Supra-SCNP volumetric compaction, we aimed to ascertain whether this would facilitate a higher conversion to larger macrocycles. Accordingly, a new series of libraries were prepared with a fixed concentration of **PT**$_{703}$ (15.00 mM, in monomer) and varying concentration of **A** to generate Supra-SCNPs at distinct folding intensities. As **A**'s concentration escalated from 0.30 mM to 7.50 mM, both the hydrodynamic radius (R_h) and the transverse relaxation time (T_2) of the Supra-SCNP diminished, indicative of a heightened folding degree and compactness (Figure 3E). Consistent with expectations, HPLC analysis revealed a proportional increase in the conversion to larger macrocycles correlating with the folding degree (Figure 3F). In comparison to control DCLs, the presence of the polymer template significantly augmented the conversion to larger macrocycles at a comparatively lower increment of **A**'s concentration, underscoring the folding-induced enhancement in local effective concentration of $\mathbf{A}_n$. This finding corroborates the notion that macrocyclic non-covalent crosslinkers dynamically adapt to their folding milieu by counterbalancing the augmented local effective concentration resulting from folding, aligning with Le Chatelier's principle.[14]

To verify the significance of this structural adaptability from the crosslinkers, **PT**$_{703}$ was interacted with small molecules analogous to $\mathbf{A}_n$. We chose benzoic acid (**BA**) and perylene-3,4,9,10-tetracarboxylic acid (**PTA**) with the same crosslinking motif of **BA** as $\mathbf{A}_n$, but with elementary motif valences and immutable chemical structures bearing no structural adaptability. Compared to molecular behaviours induced by the interaction between $\mathbf{A}_n$ and **PT**$_{703}$, neither **BA** nor **PTA** folded **PT**$_{703}$, which was confirmed by the DLS analysis, DOSY 2D plots and T_2 measurements (Figure S15 and Figure S17, Table. S3). Moreover, according to the DOSY 2D plots, NOESY and T_2 measurements (Figure S17 and S18, Table. S3), the binding between the analogous crosslinkers and **PT**$_{703}$ was undetectable or weak. The more detailed data analysis has been shown in the support information (Materials and Methods, Figure S15–S18 and Table. S3). These results demonstrated the significance of the structural adaptability in the crosslinkers to drive efficient binding and folding on the polymer.

Interactive synchronisation of Self-Adaptive Synthesis and Dynamic Folding

Upon clarifying the spatial distribution and amplification mechanism of non-covalent crosslinkers within Supra-SCNPs at equilibrium, our investigation proceeded to the

synchronized dynamics of self-adaptive synthesis and polymer folding.

First, we need to profile both the DCC and folding kinetics synchronously in a library until the dual equilibrium. To achieve this, we monitored the kinetics of compositional changes of $\mathbf{A}_n$ in the 3**A**-15$\mathbf{PT}_{703}$ library using HPLC. Simultaneously, the folding kinetics of the polymer template was tracked by DOSY (Figure 4A, Figure S19).

At the beginning when the library was prepared, **A** already bound to $\mathbf{PT}_{703}$ quantitatively, evidenced by their common *D* determined by DOSY (Figure S20), suggesting the interactive dynamics between two processes from the start. As the oxidation progressed, $\mathbf{A}_3$ and $\mathbf{A}_4$ emerged as the primary and secondary products, respectively, up to 200 hours after preparing the library. In parallel, the R_h of $\mathbf{PT}_{703}$ decreased and reached a plateau, indicating a kinetic intermediate state. At this stage, as the thiol almost entirely consumed, the disulfide-disulfide exchange reaction initiated the conversion from $\mathbf{A}_3$ and $\mathbf{A}_4$ to $\mathbf{A}_5$-$\mathbf{A}_{11}$. As the exchange reaction approaching equilibrium, the concentration of larger macrocycles $\mathbf{A}_5$-$\mathbf{A}_{11}$ significantly increased, dominating the production of crosslinkers. Concurrently, the size of polymer $\mathbf{PT}_{703}$ reduced and stabilized accordingly. These kinetic studies demonstrated two stages of synchronization between reversible chemical and folding process.

The first stage of synchronization was marked with the presence of thiol and dominated by the thiol-disulfide exchange. We hypothesised that the thiols inhibited the formation of $\mathbf{A}_5$-$\mathbf{A}_{11}$. If the hypothesis is correct, introducing fresh **A** to a pre-equilibrated library will transiently reverse the conversion of $\mathbf{A}_5$-$\mathbf{A}_{11}$, which will then gradually reform upon the oxidation of thiols. To verify, 0.75 mM fresh **A** was introduced to a pre-equilibrated 3**A**-15$\mathbf{PT}_{703}$ library (Figure 4B). Indeed, the larger macrocycles $\mathbf{A}_5$-$\mathbf{A}_{11}$ were almost quantitatively converted to $\mathbf{A}_3$ right after the addition. Then the gradual conversion from $\mathbf{A}_3$ to $\mathbf{A}_5$-$\mathbf{A}_{11}$ followed the oxidation of free thiols. Moreover, we testified the instant dual equilibrium after mixing pure $\mathbf{A}_3$ or $\mathbf{A}_4$ (3.00 mM, in **A**) with 15.00 mM $\mathbf{PT}_{703}$ by examining the chemical equilibrium by HPLC and folding equilibrium by DOSY (Figure S21). The libraries prepared by these two mixing procedures instantly reached the same $\mathbf{A}_n$ distribution and *D* as the reference library equilibrated from mixing fresh **A** and $\mathbf{PT}_{703}$, and no longer changed, indicating reaching the same dual equilibrium. It validated the premise that $\mathbf{A}_3$ and $\mathbf{A}_4$ binding to the polymer inherently promoted the dual

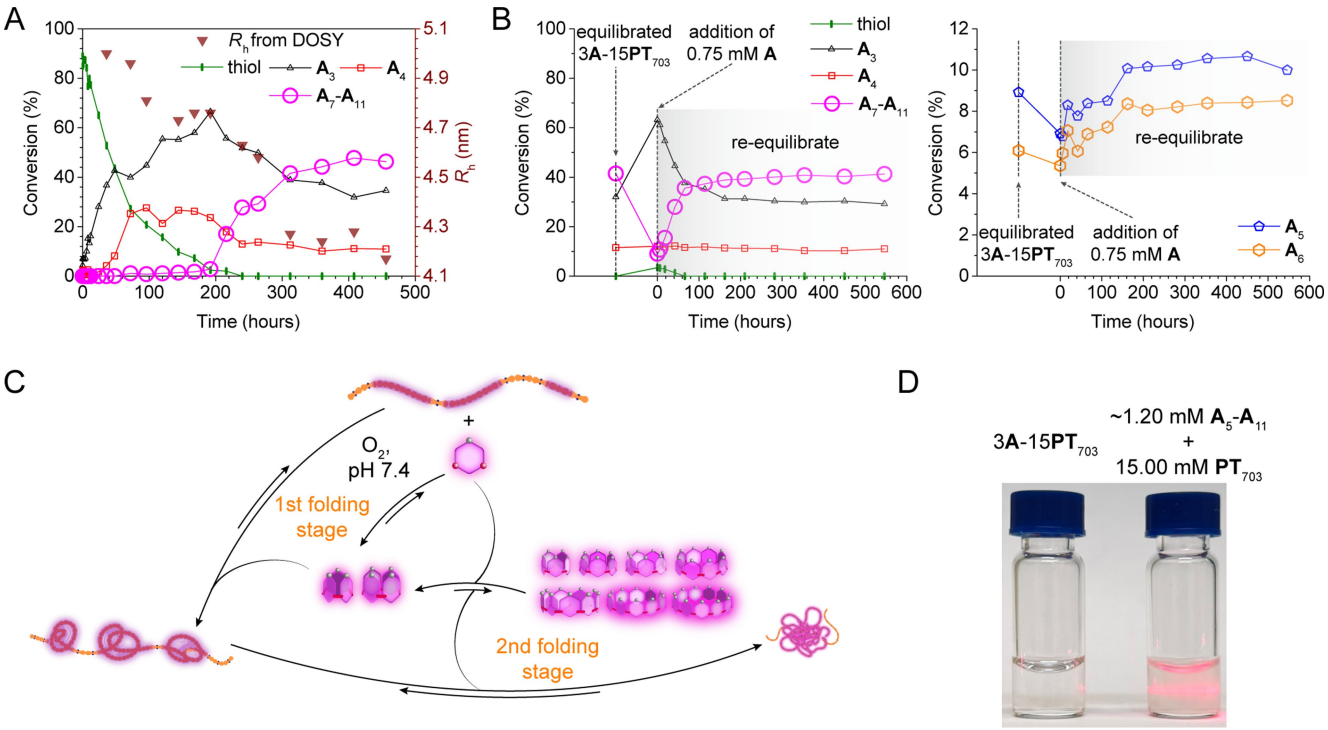

Figure 4. (**A**) Kinetic monitoring of the **A**'s conversion percentage into the macrocycle species (analysed from HPLC spectra) and the R_h (derived from *D* in DOSY) of the polymer-macrocycle complex in the 3**A**-15$\mathbf{PT}_{703}$. The sample was prepared in deuterated phosphate buffer at pD 7.4. (**B**) The thiol-disulfide exchange experiment operated by adding fresh 0.75 mM **A** (25 mol%) to a pre-equilibrated 3**A**-15$\mathbf{PT}_{703}$ DCL. Immediately after the addition, the kinetics of the compositional change of $\mathbf{A}_n$ in the DCL was monitored by HPLC. (**C**) Schematic of the synthetic process of Supra-SCNPs from the very initial point of both DCC and folding. In the first stage, the oxidation of thiol was the rate-determining process. By rapid thiol-disulfide exchange, the presence of the free-thiol-bearing **A**&$\mathbf{A}_2$ would efficiently suppress the production of the larger macrocycles of $\mathbf{A}_5$-$\mathbf{A}_{11}$. In the second stage, without the extensive impact from thiol-disulfide exchange, the as-synthesized and bound $\mathbf{A}_3$&$\mathbf{A}_4$ underwent rapid disulfide-disulfide exchange under folding to convert to their larger forms of $\mathbf{A}_5$-$\mathbf{A}_{11}$ and completed the synthesis of Supra-SCNPs. (**D**) Comparison of the Tyndall phenomenon between the Supra-SCNP solution of 3**A**-15$\mathbf{PT}_{703}$ and the aggregated mixture of ~1.20 mM the ensemble of $\mathbf{A}_5$- $\mathbf{A}_{11}$ and 15.00 mM $\mathbf{PT}_{703}$.

equilibrium by disulfide-disulfide exchange, yet free thiols prevented the synthesis of $\mathbf{A}_5$-$\mathbf{A}_{11}$ and folding progression by thiol-disulfide exchange.

Notably, the second phase's kinetic profile suggested a catalytic synchronization between DCC and folding. It was primarily indicated by the sigmoidal transition from $\mathbf{A}_3$ and $\mathbf{A}_4$ to $\mathbf{A}_5$-$\mathbf{A}_{11}$. Since $\mathbf{A}_3$ and $\mathbf{A}_4$ were probed with stronger dynamics and hydrophilicity than $\mathbf{A}_5$-$\mathbf{A}_{11}$ when binding with $\mathbf{PT}_{703}$ (Figure 2C and **S14**), we reasoned that the binding of $\mathbf{A}_3$ and $\mathbf{A}_4$ would not only introduce hydrophobic effect by charge neutralisation, but also catalyse the chain rearrangement from the initial aqueous environment, making it kinetically accessible to the folding that formed the hydrophobic core. In turn, the hydrophobic core amplified $\mathbf{A}_5$-$\mathbf{A}_{11}$ at the consumption of $\mathbf{A}_3$ and $\mathbf{A}_4$ governed by the Le Chatelier's principle, marked as a local energy minimum for synchronisation. As a result, $\mathbf{A}_3$ and $\mathbf{A}_4$, when being synchronised with template folding, worked as both reactants and catalysts for their own reaction to $\mathbf{A}_5$-$\mathbf{A}_{11}$ (Figure 4 C). Along with the continued folding and consumption of $\mathbf{A}_3$ and $\mathbf{A}_4$ during this synchronisation, the concentration of reactant and catalytic activity both dropped, which resulted the sigmoidal kinetic profile toward equilibrium.

Additionally, though sharing the similar sigmoidal synthetic profile, this catalytic synchronisation toward thermodynamic equilibrium differed from the self-catalytic replicators in out-of-equilibrium systems.[15] Self-replications are more akin to biological reproduction. Catalytic synchronisation between DCC and folding, through its critical dependence on the timing of product formation, more closely mirroring biotic peptide folding introduced earlier. The criticality of timing was probed by isolating a mixture of $\mathbf{A}_5$-$\mathbf{A}_{11}$ from a balanced 3**A**-15$\mathbf{PT}_{703}$ library via preparative HPLC, subsequently introducing it to $\mathbf{PT}_{703}$ (15.00 mM). Contrary to Supra-SCNP formation, precipitation observed (Figure 4D), presumably due to robust interchain interactions facilitated by $\mathbf{A}_5$-$\mathbf{A}_{11}$'s affinity for the polymer. Coupled with previous NOESY, DOSY and T_2 analysis indicating $\mathbf{A}_3$ and $\mathbf{A}_4$ being on the outer shell of the Supra-SCNPs, we hypothesised that the bound $\mathbf{A}_3$ and $\mathbf{A}_4$ on polymer also worked as surfactants for the hydrophobic core. Indeed, when we mixed $\mathbf{A}_3$ and $\mathbf{A}_4$ together with the larger ones $\mathbf{A}_5$-$\mathbf{A}_{11}$ and the polymer, the dual equilibrium was reached instantly (Figure S21).

These findings demonstrated the synchronized adaptive synthesis of non-covalent crosslinkers $\mathbf{A}_n$ and the folding process, which guaranteed the efficient thermodynamic folding control: $\mathbf{A}_3$ and $\mathbf{A}_4$ preorganised the polymer into an intermediate and single-chain state, catalysing the folding, and folding further facilitated the disulfide-disulfide exchange reaction from $\mathbf{A}_3$ and $\mathbf{A}_4$ to $\mathbf{A}_5$-$\mathbf{A}_{11}$, thus stabilising the folding and Supra-SCNP formation (Movie. S1). Without the pre-organization of $\mathbf{A}_3$ and $\mathbf{A}_4$, the stabilized binding and hydrophobic folding between $\mathbf{A}_5$-$\mathbf{A}_{11}$ and $\mathbf{PT}_{703}$ would inevitably happen at an inter-chain level, thus leading to inter-chain aggregation instead of single-chain folding.

Control the Self-Adaptive Synthesis and Folding for Potential Applications

This understanding spurred our exploration into how the integration of external functional molecules could modulate the adaptive synthesis and enable the functional emergence of Supra-SCNPs. Given the hydrophobic-driven folding mechanism, we hypothesized hydrophobic anti-cancer drugs, such as doxorubicin (DOX), could be accommodated within Supra-SCNPs through an adaptive folding process, marking significant strides toward drug delivery systems (DDSs). Moreover, the swift attainment of thermodynamic equilibrium, in the absence of unreacted thiols, underscores a strategic approach for preventing drugs from denaturing during the fabrication process of DDSs.

Experimentally, DOX was homogenized with 15 mM $\mathbf{PT}_{703}$ at a final concentration of 2.3 mM. The solution was then mixed with a pre-equilibrated DCL made by 3.00 mM **A** to reach the equilibrium instantly, ensuring the maximum drug loading content (DLC) of the Supra-SCNPs loaded with fresh DOX (Supra-SCNP-DOX). Using HPLC-MS, the DLC of the Supra-SCNP-DOX was determined as 22 % with a loading efficiency of 86 % and no side product was found than the macrocycles and DOX (Figure S22A). Interestingly, $\mathbf{A}_3$ was more amplified in Supra-SCNP-DOX, which proposed an adaptive enlarging of folding after loading the cargo molecules since he low-degree folding favored $\mathbf{A}_3$. Indeed, the TEM and DLS results suggested that the average R_h of the Supra-SCNP-DOX was increased to approximately 33 nm (Figure S22B and C). These results clearly suggest that we can use the external molecules to control the self-adaptive folding of the Supra-SCNP-DOX synthesized from DCLs.

Advancing to practical applications, we evaluated the potential of Supra-SCNP-DOX as a DDS. Acknowledging the elevated glutathione (GSH) levels and the lower intracellular pH (~5.6) characteristic of cancer cells,[16] we posited that such conditions would facilitate the disassembly of Supra-SCNP-DOX by reducing the disulfide bonds and protonating the carboxylate groups, enabling the release of encapsulated drugs. The hypothesis was confirmed as DOX release from Supra-SCNP-DOX was significantly expedited under reductive or acidic conditions (Figure 5A), showcasing the system's responsive drug delivery capability.

Assessing the biosafety of Supra-SCNP-DOX, we conducted in vitro cytotoxicity tests against multi-drug-resistant ovarian cancer cells (NCI/RES-ADR). The Supra-SCNP-DOX displayed markedly superior anti-cancer efficacy compared to free DOX and the polymer-DOX mix at equivalent concentrations (Figure 5B). Interestingly, among all the dosing configurations, Supra-SCNPs exhibited minimal cytotoxicity, while polymer's inherent toxicity was even more significant than the polymer-DOX mix (Figure 5C), underscoring the safety of the carrier component, and emphasising the Supra-SCNP's enhanced drug delivery efficacy against drug-resistant cancer. Flow cytometry and confocal laser scanning microscopy (LCSM) further validated the superior drug delivery efficiency of Supra-SCNP-DOX, indicating a substantial uptake of DOX by cancer

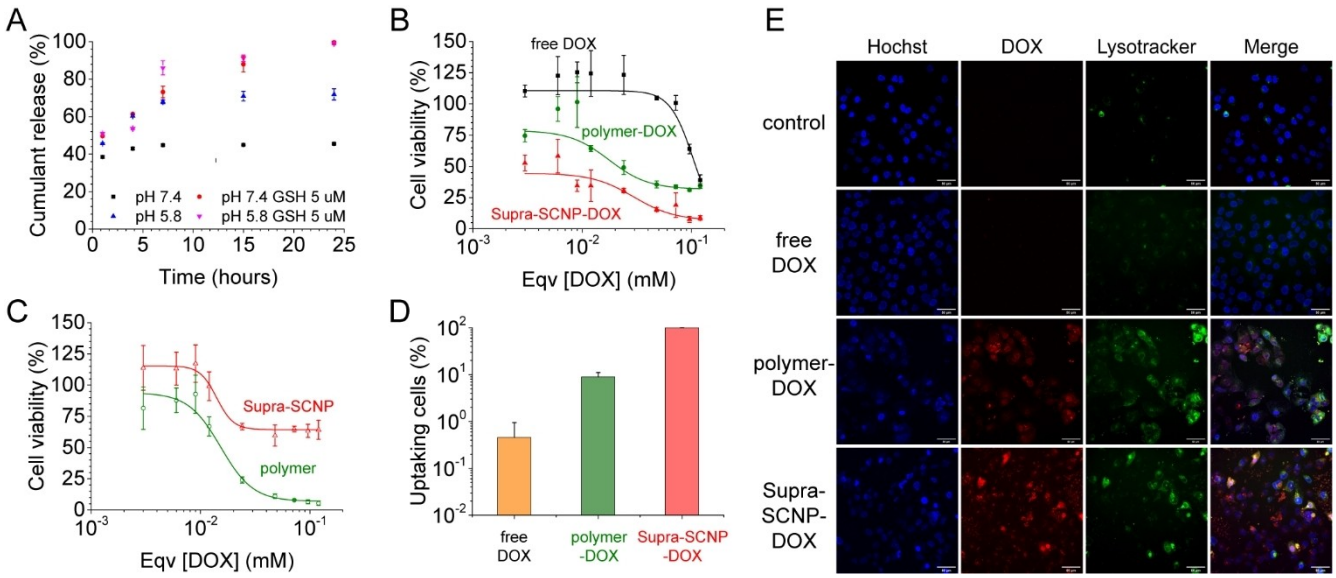

Figure 5. (**A**) Release profile of DOX from SCNP-DOX in phosphate buffers with physiological/acidic pH and absent/present GSH condition, monitored and analyzed by HPLC (standard error, $n=3$). (**B**) Cytotoxicity test of the DOX in different dose forms at 24 h (standard error, $n=6$). CCK-8 assay was used to determine the cell viability. Supra-SCNP-DOX was diluted from the original concentration after equilibrium. Dose of free DOX and polymer-DOX were directly prepared from the highest concentration shown from the plot. (**C**) Cytotoxicity test of Supra-SCNP and $\mathbf{PT}_{703}$ at 24 h (standard error, $n=6$). (**D**) Flow cytometry characterizing the percentage of cells that uptake the DOX in different dose forms after 4 hours' co-incubation (standard error, $n=3$). (**E**) LCSM visualizing the internalization of the DOX in different dose forms after 4 hours' co-incubation. The Hoechst and lysotracker channel in blue and green marked the area of the stained cell nucleus and lysosomes in the cells respectively. The DOX channel in red were detected by the inherent fluorescence of DOX to see where the DOX molecules were located. And the three channels were merged to allow co-localization of the different stained components.

cells (Figure 5D and E), thereby affirming the system's efficacy in overcoming drug resistance through optimized drug delivery.

Conclusions

Leveraging DCC, we have engineered self-adaptive non-covalent crosslinkers that fold synthetic polymers in a synchronised manner. This method harnesses reversible reactions to create macrocycles that restructure themselves in real-time to guide the folding through intermediate states towards the equilibrium. Introducing DOX as a folding modulator enabled the synthesis of enlarged Supra-SCNP-DOX without side reactions or drug denaturation, enhancing the drug potency against drug-resistance cancer cells by improving drug delivery efficiency. Our study synchronizes polymer folding with self-adaptive synthesis from DCC, enriching the domain of DCC by elucidating species evolution guided by the structural dynamics of folding polymers. This innovative integration not only advances our understanding of stepwise synthetic polymer folding into Supra-SCNPs but also paves the way for emulating the complex functionalities inherent to proteins.

Supporting Information

The authors have cited additional references within the Supporting Information (Ref. [17]).

Acknowledgements

We are grateful for the financial support from the Sigrid Jusélius Foundation (Senior Researcher Fellowship for J.L.) and the Academy of Finland (decision no. 318524, project funding for J.L.). We thank the Electron Microscopy Laboratory, Institute of Biomedicine, University of Turku, and Biocenter Finland for providing TEM services. The facilities and expertise of the HiLIFE NMR unit at the University of Helsinki, a member of Instruct-ERIC Centre Finland, FINStruct, and Biocenter Finland are gratefully acknowledged for their NMR services. We thank the Turku Centre for Chemical and Molecular Analytics (CCMA), Turku, Finland, for providing NMR and LC–MS services. We thank OtaNano Nanomicroscopy Center, Aalto University, Finland and The Paul Scherrer Institute (PSI), Würenlingen, Switzerland, for providing SAXS and cSAXS measurements. We thank the School of Chemical Engineering, Aalto University, Finland for providing SEC measurements. Dr. Xue Zhang at Max Planck Institute of Colloids and Interfaces, Germany is acknowledged for her assistance for the SEC and refractive index measurement. We thank Dr. Jia Li from the Radiology department, Beijing Friend-

ship Hospital, Beijing, China for his generous donation of anti-cancer drugs and consumables for confocal microscopy.

Conflict of Interest

The authors declare no conflict of interest.

Data Availability Statement

The data that support the findings of this study are available from the corresponding author upon reasonable request.

Keywords: dynamic combinatorial chemistry · supramolecular chemistry · polymer folding · single-chain nanoparticle

[1] a) D. A. Liberles, S. A. Teichmann, I. Bahar, U. Bastolla, J. Bloom, E. Bornberg-Bauer, L. J. Colwell, A. P. J. de Koning, N. V. Dokholyan, J. Echave, A. Elofsson, D. L. Gerloff, R. A. Goldstein, J. A. Grahnen, M. T. Holder, C. Lakner, N. Lartillot, S. C. Lovell, G. Naylor, T. Perica, D. D. Pollock, T. Pupko, L. Regan, A. Roger, N. Rubinstein, E. Shakhnovich, K. Sjölander, S. Sunyaev, A. I. Teufel, J. L. Thorne, J. W. Thornton, D. M. Weinreich, S. Whelan, *Protein Sci.* **2012**, *21*, 769–785; b) D. Pal, D. Eisenberg, *Structure* **2005**, *13*, 121–130.

[2] a) C.-C. Cheng, F.-C. Chang, H.-C. Yen, D.-J. Lee, C.-W. Chiu, Z. Xin, *ACS Macro Lett.* **2015**, *4*, 1184–1188; b) S. Mavila, O. Eivgi, I. Berkovich, N. G. Lemcoff, *Chem. Rev.* **2016**, *116*, 878–961; c) M. ter Huurne Gijs, R. A. Palmans Anja, E. W. Meijer, *CCS Chemistry* **2019**, *1*, 64–82; d) M. A. M. Alqarni, C. Waldron, G. Yilmaz, C. R. Becer, *Macromol. Rapid Commun.* **2021**, *42*, 2100035.

[3] a) R. J. Ellis, S. M. J. A. r. o. b. Van der Vies, **1991**, *60*, 321–347; b) F. U. Hartl, A. Bracher, M. Hayer-Hartl, *Nature* **2011**, *475*, 324–332.

[4] a) L. Ellgaard, N. McCaul, A. Chatsisvili, I. Braakman, *Traffic* **2016**, *17*, 615–638; b) Nitika, C. M. Porter, A. W. Truman, M. C. Truttmann, *J. Biol. Chem.* **2020**, *295*, 10689–10708.

[5] a) N. Hosono, M. A. J. Gillissen, Y. Li, S. S. Sheiko, A. R. A. Palmans, E. W. Meijer, *J. Am. Chem. Soc.* **2013**, *135*, 501–510; b) A. J. Moreno, F. Lo Verso, A. Sanchez-Sanchez, A. Arbe, J. Colmenero, J. A. Pomposo, *Macromolecules* **2013**, *46*, 9748–9759; c) F. Lo Verso, J. A. Pomposo, J. Colmenero, A. J. Moreno, *Soft Matter* **2014**, *10*, 4813–4821; d) A. Blazquez-Martín, E. Verde-Sesto, A. J. Moreno, A. Arbe, J. Colmenero, J. A. Pomposo, *Polymers* **2021**, *13*.

[6] a) J.-M. Lehn, A. V. Eliseev, *Science* **2001**, *291*, 2331–2332; b) J. N. Reek, S. Otto, *Dynamic combinatorial chemistry*, John Wiley & Sons, **2010**; c) J. Li, P. Nowak, S. Otto, *J. Am. Chem. Soc.* **2013**, *135*, 9222–9239; d) C. Jia, D. Qi, Y. Zhang, K. Rissanen, J. Li, *ChemSystemsChem* **2020**, *2*, e2000019.

[7] a) A. M. Hartman, R. M. Gierse, A. K. H. Hirsch, *Eur. J. Org. Chem.* **2019**, *2019*, 3581–3590; b) A. Canal-Martín, R. Pérez-Fernández, *ACS Omega* **2020**, *5*, 26307–26315.

[8] P. Saha, D. Panda, J. Dash, *Chem. Soc. Rev.* **2023**, *52*, 4248–4291.

[9] D. Carbajo, Y. Pérez, J. Bujons, I. Alfonso, *Angew. Chem. Int. Ed.* **2020**, *59*, 17202–17206.

[10] U. Gedde, *Polymer physics*, Springer Science & Business Media, **1995**.

[11] a) S. Otto, R. L. E. Furlan, J. K. M. Sanders, *Science* **2002**, *297*, 590–593; b) P. T. Corbett, J. K. M. Sanders, S. Otto, *Chem. Eur. J.* **2008**, *14*, 2153–2166.

[12] a) L. F. Pinto, J. Correa, M. Martin-Pastor, R. Riguera, E. Fernandez-Megia, *J. Am. Chem. Soc.* **2013**, *135*, 1972–1977; b) L. F. Pinto, R. Riguera, E. Fernandez-Megia, *J. Am. Chem. Soc.* **2013**, *135*, 11513–11516; c) S. Liao, L. Wei, L. A. Abriata, F. Stellacci, *Macromolecules* **2021**, *54*, 11459–11467; d) M. Nagao, Y. Miura, *ACS Macro Lett.* **2023**, *12*, 733–737.

[13] a) H. L. J. C. R. A. d. S. Le Chatelier, **1884**, *99*, 786–789; b) J. De Heer, *J. Chem. Educ.* **1957**, *34*, 375; c) W. Lin, C. J. Murphy, *ACS Cent. Sci.* **2017**, *3*, 1096–1102.

[14] It is worth noting that compared to $\mathbf{A}_3$ and $\mathbf{A}_4$, $\mathbf{A}_n$ in larger sizes ($n \geq 5$) may have higher binding affinity to the compactly folded polymer segments. However, the dynamic nature of these compact polymer segments makes it impossible to purify them and determine binding constants through titration experiments. Consequently, while we have not discussed the amplification of larger macrocycles due to stronger binding, this possibility cannot be ruled out.

[15] P. Adamski, M. Eleveld, A. Sood, Á. Kun, A. Szilágyi, T. Czárán, E. Szathmáry, S. Otto, *Nat. Chem. Rev.* **2020**, *4*, 386–403.

[16] a) G. K. Balendiran, R. Dabur, D. Fraser, *Cell Biochem. Funct.* **2004**, *22*, 343–352; b) B. A. Webb, M. Chimenti, M. P. Jacobson, D. L. Barber, *Nat. Rev. Cancer* **2011**, *11*, 671–677.

[17] V. Yarlagadda, P. Akkapeddi, G. B. Manjunath, J. Haldar, *J. Med. Chem.* **2014**, *57*, 4558–4568.

Manuscript received: May 7, 2024
Accepted manuscript online: June 29, 2024
Version of record online: ■■, ■■

Research Article

Polymer Chemistry

D. Qi, X. Shi, C. Lin, F. Holzhausen, L. Ville, X. Sun, J. Luo, L. Pitkänen, Y. Zhu, J. Rosenholm, S. Jalkanen, J. Li* ——— **e202408670**

Self-Adaptive Synthesis of Non-Covalent Crosslinkers while Folding Single-Chain Polymers

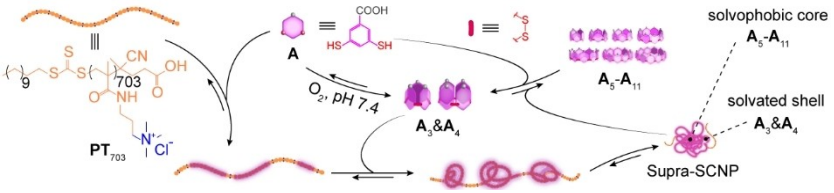

Dynamic combinatorial macrocyclic disulfides acted as non-covalent crosslinkers, adapting to polymer folding. Initially, small macrocycles fold the polymer into a loose state, which then catalysed the formation of larger macrocycles to enhance folding efficiency. Our work deepens the understanding of interplay between adaptive synthesis and dynamic folding, advancing the strategy for replicating protein folding into functional nanoparticles.